ACS APPLIED MATERIALS & INTERFACES

Letter

www.acsami.org

Site-Selective Ion Beam Synthesis and Optical Properties of Individual CdSe Nanocrystal Quantum Dots in a SiO_2 Matrix

H. Moritz Mangold,[†] Helmut Karl,[‡] and Hubert J. Krenner*[,†,§,⊥]

[†]Emmy Noether Junior Reserach Group at Lehrstuhl für Experimentalphysik 1 and Augsburg Centre for Innovative Technologies (ACIT), Universität Augsburg, Universitätsstraße 1, 86159 Augsburg, Germany

[‡]Lehrstuhl für Experimentalphysik IV, Universität Augsburg, Universitätsstraße 1, 86159 Augsburg, Germany

[§]Center for NanoScience (CeNS), Ludwig-Maximilians-Universität München, Geschwister-Scholl-Platz 1, 80539 München, Germany

[⊥]Nanosystems Initiative Munich (NIM), Schellingstraße 4, 80799 München, Germany

Supporting Information

ABSTRACT: Cadmium selenide nanocrystal quantum dots (NC-QDs) are site-selectively synthesized by sequential ion beam implantation of selenium and cadmium ions in a SiO_2 matrix through submicrometer apertures followed by a rapid thermal annealing step. The structural and optical properties of the NC-QDs are controlled by the ion fluence during implantation and the diameter of the implantation aperture. For low fluences and small apertures the emission of these optically active emitters is blue-shifted compared to that of the bulk material by >100 meV due to quantum confinement. The emission exhibits spectral diffusion and blinking on a second time scales as established also for solution-synthesized NC-QDs.

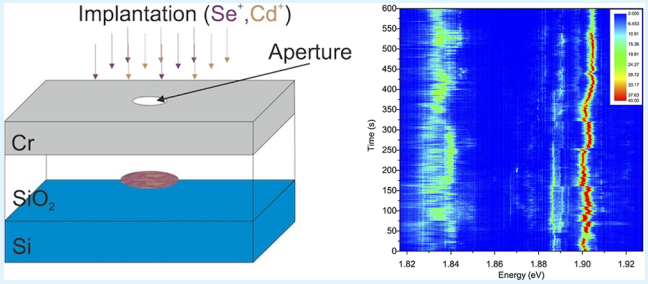

KEYWORDS: *ion beam implantation, quantum dots, glass, photoluminescence, silicon photonics, spectral diffusion*

INTRODUCTION

Ion beam implantation is a widely applied technique to modify the electronic and optical properties of semiconducting and insulating materials since it allows to incorporate any element of the periodic table in arbitrary planar, nonplanar or textured substrate.[1,2] Because it has been a key technology in the semiconductor industry for more than half a century[3−5] the massive reduction of the feature size in MOS technology over this long time span has been making high demands on this key fabrication technique. For present day integrated circuits nanofabricated implantation masks are routinely employed to confine the implantation to nanoscopic volumes. In addition to the modification of the electrical properties of materials, fluorescing defects can be incorporated for (quantum-) optical applications.[6−8] However, these defects are implanted in low concentrations and their resulting emission wavelengths are predefined by the nature of the defect. To circumvent this limitation, we can apply an alternative route to synthesize bright emitters with tunable wavelength using ion beam technology. For high dose implants nanoscale precipitates can be formed during a postimplantation annealing step[9,10] because of Ostwald ripening. The such obtained nanocrystals (NCs) are embedded in the host matrix and depending on the type of NC, the dielectric,[11,12] plasmonic[13] or optical emission properties of the such obtained nanocomposite can be tailored. In particular, ensembles of optically active NC-quantum dots (NC-QDs) of elemental semiconductors, most notably silicon,[14] and II−VI compounds[15] have been synthesized and used as active materials in photonic devices,[16−19] compatible with silicon technology. The thermally activated NC precipitation was also used to form optically active II−VI compound NC-quantum dots (NC-QDs) in a glass matrix doped with the individual elements.[20] Experiments performed on these bright emitters opened a new field of fundamental and applied research on NC-QDs. Because monodisperse NC-QDs can be synthesized in solutions,[21] intentionally doped with impurities, novel opto-electronic,[22] biomedical,[23] and photovoltaic applications[24] came within reach. One distinct advantage of solution synthesized NC-QDs is their straightforward embedding into large volume matrix and NC-QD-glass composites have in the meantime found practical application in consumer electronics. However, site-selective hybridization of a complex host matrix with individual solution synthesized NC-QDs is extremely challenging. To realize such hybrid systems, which would be particularly suited for example, for NC-QD single photon sources[25] on a silicon compatible architecture, ion beam synthesis in SiO_2 performed through nanofabricated apertures provides a direct and elegant approach toward single NC-QDs devices. Because of their full and coherent encapsulation within the SiO_2 matrix,

Received: September 26, 2013
Accepted: January 22, 2014
Published: January 22, 2014

   dx.doi.org/10.1021/am404227x | ACS Appl. Mater. Interfaces 2014, 6, 1339−1344

ion-beam-synthesized NC-QDs exhibit long-term stability without photobleaching.

In this letter, we report on the synthesis of individual, optically active cadmium selenide (CdSe) NC-QDs by sequential ion beam implantation through submicrometer implantation masks followed by a short rapid thermal annealing step. We show that the combination of low ion fluences and feature sizes smaller than 1000 nm can be readily used to synthesize small diameter NC-QDs with quantum confined electronic states at low areal density. These NC-QDs exhibit sharp spectral lines which can be tuned spectrally during fabrication by the implantation aperture diameter. Single NC-QD emission lines exhibit both spectral diffusion and blinking (intermittency), which are characteristic fingerprints also observed for their colloidal counterparts.

EXPERIMENTAL SECTION

The experimental procedure to synthesize CdSe NCs is presented in panels a and b in Figure 1 and consists of two

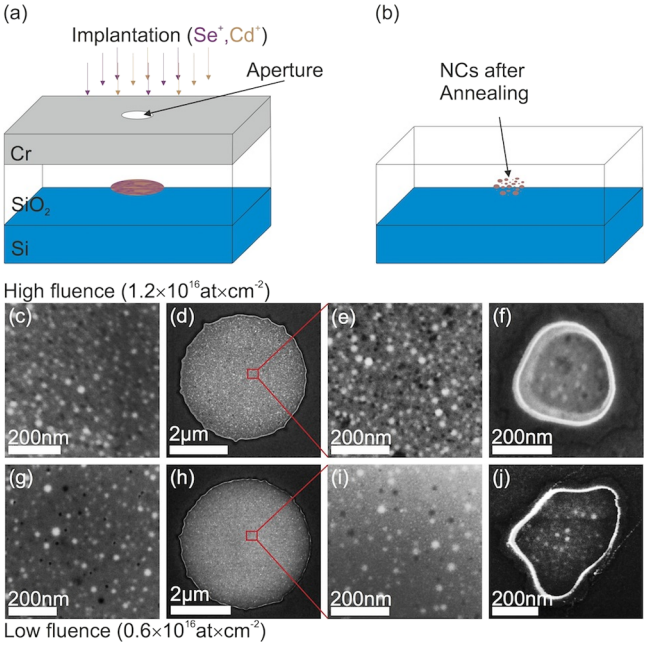

Figure 1. Synthesis and SEM characterization: (a, b) Schematic of site-selective ion beam synthesis through submicrometer apertures. SEM images of high (upper row) and low fluence (bottom row) samples from (c, g) unpatterned regions, (d, e, h, i) large apertures, and (f, j) small apertures.

major steps. First, implantation apertures are defined by electron beam lithography and wet chemical etching in a 120 nm thick chromium mask, evaporated on the 200 nm thick thermal oxide on a commercial Si wafer. The diameters of these apertures (d) ranged between d = 400 nm to d = 4500 nm. An unpatterned region without a Cr mask provides a reference on the same substrate. For the experiments presented here, we prepared 8 mm ×5 mm substrates which contained a ~3 mm × 5 mm wide unpatterned reference stripe. In the following, Se^+ followed by Cd^+ ions were implanted at cryogenic temperature (77 K) in SiO_2 with energies of 134 kV, and 190 kV, respectively as shown in Figure 1a. These energies give rise to Gaussian concentration profiles for both ion species centered at a projected range of 100 nm below the sample surface. Here we present results from two different substrates implanted during the same steps with ion fluences of $F_0 = 0.6 \times 10^{16}$ at/cm^2 and $2F_0$. We precisely controlled these fluences by blanking the beam using a house built shutter assembly.[10] We refer to these samples as the low and high fluence sample in the following. Taking into account the ~60 nm width of the implantation profiles, these ion fluences correspond to an overall incorporation of Cd and Se of $n_{Cd} = n_{Se} = 1 \times 10^{21}$ cm^{-3}. In addition to the incorporation of ≥1 at % material, the short-range order in the amorphous matrix is destroyed by the ion beam bombardment, giving rise to a increase in the structural defect density. Moreover, we want to note that these fluences are significantly reduced compared to previous work in which no indications of a quantum confined level structure has been observed because of a large NC size.[18] In the second and final step depicted in Figure 1b, the Cr implantation mask is removed by wet chemical etching and NCs are formed during a post implantation rapid thermal annealing (RTA) step at 900 °C for 30 s. The formation of CdSe NC in the unpatterned regions and within the apertures was confirmed by Raman spectroscopy. In the spectra included in the Supporting Information, we resolved the characteristic LO phonon mode of CdSe in the implanted areas. To ensure full comparability, both samples were implanted during the same runs and NCs are formed during the same RTA step.

We characterized the such synthesized NCs samples by scanning electron microscopy (SEM). Typical micrographs from an unpatterned region are compared to that from large and small apertures in Figure 1c–f (high fluence sample) and g–j (low fluence sample). In images d, f, h, and j, the implanted areas are clearly resolved as bright regions because of the improved contrast of the CdSe-SiO_2 composite. Individual NCs (bright) and voids (black) are clearly visible at high magnification in unpatterned regions in c and g, inside large $d \approx 4000$ nm apertures in e and i, and in the micrograph recorded from submicrometer apertures in g and j. NCs and voids can be distinguished because of the different contrast that arises from a build up of persistent charge at the unpassivated SiO_2 surface of the voids. The latter naturally occur because of evaporation of highly nonstoichiometric clusters. A representative TEM image of a reference sample showing both NCs and voids is included in the Supporting Information.

In contrast to these pronounced signatures in the implanted areas, we do not resolve any modification of the SiO_2 in regions protected by the Cr mask, proving the site-selectivity of our approach. We want to note that a full quantitative analysis of the NC density and size distribution would require time-consuming TEM preparation and analysis in the implanted regions. Nevertheless, our straightforward plan-view SEM analysis allows us to estimate the NC density and derive trends in the variation of the average NC size.

The high-magnification images from unpatterned regions presented in Figure 1c, g and in the Supporting Information demonstrate that the areal density of NCs (bright) reduces from 320 ± 50 μm^{-2} for the high fluence to 200 ± 50 μm^{-2} for the low fluence sample. This reduction is expected because of the reduced amount of Cd and Se introduced.

For large diameter apertures (cf. Figure 1e, i and the Supporting Information), the NC density reduces to 280 ± 50 μm^{-2} and 160 ± 50 μm^{-2} for the high and low fluence sample, respectively. When further decreasing the aperture size, the micrographs in Figure 1f, j show that the average NC size decreases for both fluences. In particular, for the low fluence

dx.doi.org/10.1021/am404227x | ACS Appl. Mater. Interfaces 2014, 6, 1339–1344

sample, NC diameters range at or below the spatial resolution of SEM. These findings provide a first indication that the spatial confinement of the implantation area gives rise to a pronounced modification of the NC formation during the RTA step.

The optical properties of our ion beam synthesized NCs reflect their structural size as established for their chemically synthesized QD counterparts.[21,26,27] We studied the optical emission of our NCs by conventional low-temperature microphotoluminescence (PL). The sample was mounted on the coldfinger of a He-flow cryostat (T = 8.5 K) and carriers were photogenerated by a continuous wave diode laser (λ_{Laser} = 405 nm) focused to an ~1 μm diameter spot. The PL-emission was collected and dispersed by a 0.5 m single grating monochromator and detected by a cooled Si CCD detector. We start by evaluating the ensemble optical properties of these ion beam synthesized NCs. We assess the ensemble optical properties of NC through $d \leq 1200$ nm diameter openings by summing spectra recorded from 5 (high fluence sample) and 10 individual (low fluence sample) apertures of identical diameter. The individual spectra are included in the Supporting Information. All PL spectra in Figure 2 are normalized to the maximum intensity of the NC emission and the low temperature band gap of bulk CdSe of $E_{gap,bulk}$ = 1.839 eV (T = 8.5 K) is marked by vertical green lines.

In Figure 2, we compare the PL of the low and high fluence sample from unpatterened regions (a, b) to that of NCs synthesized through large d = 4350 nm (c, d) and small diameter, d = 420 nm (e, f), apertures. In all regions we detect emission centered close to the $E_{gap,bulk}$ of CdSe. This emission is

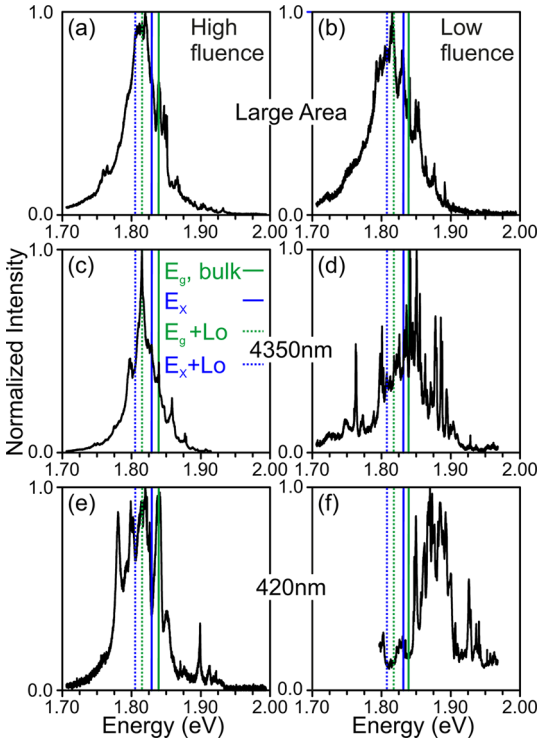

Figure 2. Ensemble optical properties: Normalized μ-PL spectra from the high (left) and low (right) fluence samples recorded from (a, b) unpatterned regions, (c, d) large apertures and (e, f) small apertures. The green and blue solid lines mark the bulk CdSe bandgap and the expected exciton transition, respectively. The dashed lines mark the corresponding LO-phonon replica.

detected only in the unmasked, implanted regions of the sample proving that it stems from CdSe NCs synthesized in these parts of the sample.

CdSe NCs in the unpatterned regions (cf. Figure 2a, b) exhibit broad emission peaks that are shifted to lower energies by ~25 meV with respect to $E_{gap,bulk}$. Moreover, the emission signals for the high and low fluence sample exhibit a significant broadening of 43 and 49 meV, respectively. The red shift of the NC emission with respect to the bandgap of bulk CdSe arises from a combination of different contributions, (i) excitonic corrections, (ii) LO phonon-assisted transitions, (iii) exciton localization at defects, and (iv) electronic coupling to randomly distributed and charged defects in the surrounding SiO_2 matrix. We estimate the resulting energy shifts using the bulk CdSe values of the exciton binding energy, E_X = 11.6 meV and the LO phonon energy E_{LO} = 213 cm^{-1} = 26.4 meV.[28] The expected exciton emission energy is marked by the vertical solid blue line. The vertical dashed lines indicate the expected single LO phonon replica of the bulk bandgap (green) and the exciton (blue). Clearly, the observed emission energies span the range of energies expected for bulk CdSe. In addition, we expect further energy renormalization which manifests itself in a broadening of the emission peak: On the one hand, shifts to lower energies can be readily explained, for example, by exciton localization at internal and interface defects, interaction with defects in the surrounding SiO_2, and higher-order phonon replica. On the other hand, quantum confinement effects in small NCs to first order always gives rise to a blue shifts of the exciton transition.

For NCs synthesized by site-selective implantation through apertures, we observe dramatically different emission characteristics for the high and low fluence sample. The PL signal of the high fluence sample remains shifted to lower energies compared to $E_{gap,bulk}$ for both aperture sizes. For all three sets of data of the high fluence sample, only weak PL is detected at the high energy side of these spectra, $E > E_{gap,bulk}$, where we expect transitions from NCs exhibiting quantum confined, QD-like energy levels (NC-QDs). A close examination of the spectra indeed reveals weak signatures of sharp PL lines in the unpatterned region, Figure 2a, and d = 4350 nm, Figure 2c. For the smallest implantation aperture size, d = 420 nm, Figure 2e, the sum spectrum starts to break up in individual sharp lines at $E \approx 1.9$ev $> E_{gap,bulk}$. In contrast, the NC emission of the low fluence sample gets strongly modified when ion implantation is performed through an aperture. For the largest apertures studied, d = 4350 nm, Figure 2d, the emission is centered close to the bulk band gap of CdSe at E = 1.84 eV $\approx E_{gap,bulk}$. The modification of the NC formation leading to this pronounced energy shift might arise from a greatly enhanced diffusion of Cd and Se within the SiO_2 matrix. The diffusion length can exceed that typical for a low impurity concentrations, which is on the order of several tens of nanometers. Such an enhanced diffusion within the implanted area could be induced by high concentrations of the diffusion species and the structural defects because of destruction of the short-range order by the ion irradiation. Furthermore, the nucleating NCs form attractive sites for the implanted species and influence their diffusive transport. A detailed investigation of the underlying processes is a current work in progress and goes beyond the scope of this Letter.

The most important and most remarkable modification of the ensemble emission is observed for the smallest aperture size, d = 420 nm, on the low fluence sample. In the sum

spectrum shown in Figure 2f, the ensemble emission peak is centered at E = 1.88 eV. Despite its finite width of ∼35 meV, the ensemble peak is shifted completely above $E_{gap,bulk}$. In both data sets of NCs synthesized through apertures at low ion fluence, discrete emission lines are resolvable despite the fact that we summed spectra from 10 different apertures. This shift of the full ensemble peak which consists of sharp emission lines provides evidence that the detected emission stems from quantum confined NC-QDs.

To further support these conclusions, we performed a detailed investigation of the impact of the aperture diameter (d) on the NC emission properties. In Figure 3, we present a series

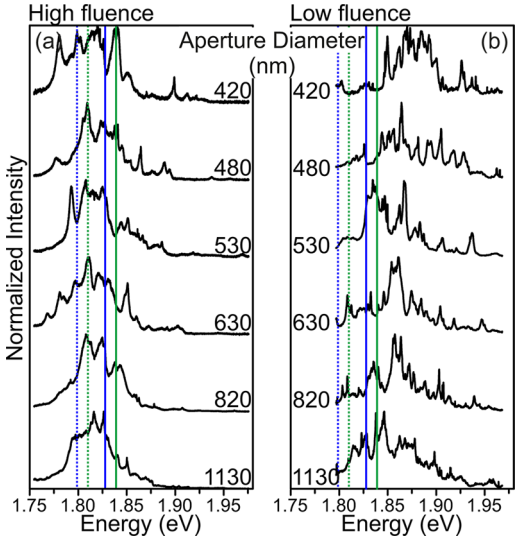

Figure 3. Ensemble optical properties for submicrometer apertures: Normalized, ensemble averaged μ-PL spectra from the high (left) and low (right) fluence samples recorded from aperture diameters ranging from d = 430−1130 nm. Data are summed from 5 and 10 implantation sites on the high and low fluence sample, respectively. The bulk band gap energy of CdSe at T = 8.5 K is marked by vertical green lines. The red (blue) lines mark the center of the ensemble emission in the unpatterned region (for d = 420 nm apertures).

of summed NC spectra of the high (a, 5 spectra) and low (b, 10 spectra) fluence sample for different aperture diameters decreasing from d = 1130 nm to d = 420 nm from the bottom to top spectra. In these plots, the expected bulk bandgap (green) and exciton (blue) transition energies (solid lines) and their LO phonon replica (dashed lines) are marked. Comparing the evolution of the NC emission with decreasing d two pronounced differences become apparent between the high and low fluence sample. The ensemble emission of the high fluence sample stays almost constant and centered at $E \approx$ 1.82 eV. For $d \leq$ 630 nm, a weak tail and individual, discrete emission lines develop at $E > E_{gap,bulk}$. In contrast, the ensemble emission of the low fluence sample exhibit such sharp emission lines above $E_{gap,bulk}$ for all diameters studied. Furthermore, the center of the ensemble emission systematically shifts toward higher energy as d decreases.

These observations again clearly demonstrate and confirm direct control and correlation of the NCs' optical properties by variation of the total ion fluence and application of a submicrometer implantation apertures. For the high fluence sample, the majority of NCs exhibits bulk-like properties and only a small fraction of NC-QDs are formed. For the low fluence sample, the majority of NCs in the ensemble are NC-QDs when employing implantation apertures. Their mean emission energy can be controllably shifted to higher energies by decreasing d.

In the last part of this Letter, we present first optical experiments preformed on single NC-QDs of the low fluence sample. In Figure 4, we plot emission spectra recorded from a d

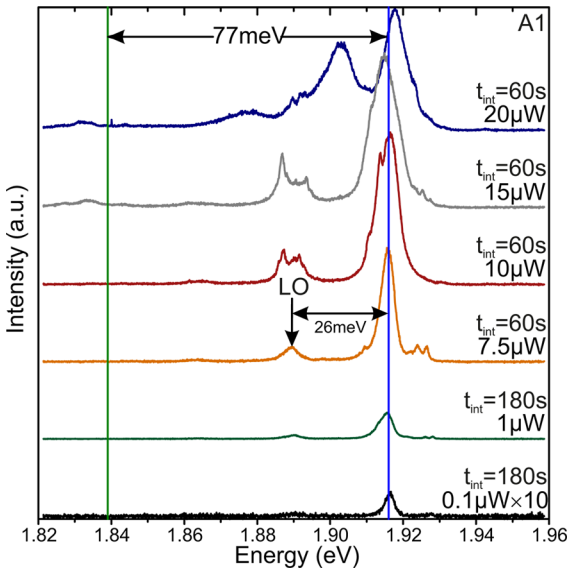

Figure 4. Single NC-QD emission: Laser-power dependent emission of a single NC-QD recorded from a d = 420 nm aperture (A1) on the low fluence sample. The LO-phonon replica of the main peak is marked by the vertical arrow.

= 420 nm aperture (A1) for different optical pump powers, increasing from P_{laser} = 100 nW (bottom spectrum) to P_{laser} = 20 μW (top spectrum). In this experiment integrations times ranged between t_{int} = 60−180 s. For low optical pump powers, the spectrum consists of a single emission line at E_0 = 1.916 eV. We attribute this emission line as arising from single exciton recombination, X, of the NC-QD. The energy shift $\Delta E_C = E_0 - E_{gap,bulk}$ = 77 meV above the bulk energy gap of CdSe suggests that this NC is in an intermediate confinement regime. The measured ΔE_C corresponds to a NC diameter of d_{NC} = 11 ± 1 nm.[29] As the optical pump power increases the peak broadens significantly and its intensity increases. Shifted by ΔE_{LO} = 26 meV toward lower energies we identify a replica of the main emission peak. This energy shift corresponds almost exactly to the LO phonon energy of bulk CdSe[28] which further supports that the detected signal is emitted from a CdSe NC-QD. At the highest pump powers the signal is spectrally shifted first to lower and finally to higher energies indicating that optical emission of these NC-QDs is sensitive to optical carrier generation rates both within the NC-QDs and in deep level defects in the SiO_2 matrix. This assumption is further supported by the relatively broad line width of fwhm ∼4 meV even at low pump powers.

Finally, we studied the temporal evolution of the optical emission of individual NC-QDs on a seconds time scale. For this experiment we selected two apertures (A2, d = 820 nm; A3, d = 630 nm) on the low fluence sample that exhibit particularly bright PL signals. These high intensities allowed for t_{int} = 1 s at P_{laser} = 20 μW (A2) and P_{laser} = 7 μW (A3). In Figure 5, we compare two 500 s time series from these apertures plotted in

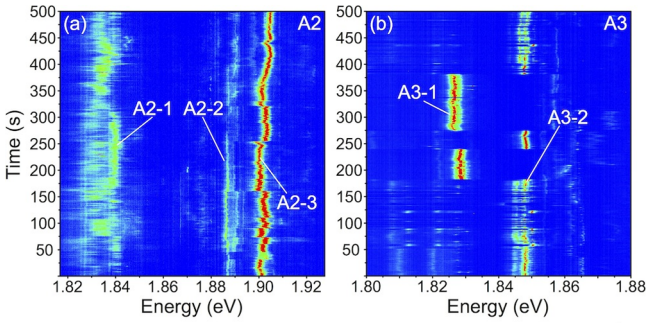

Figure 5. Spectral diffusion and intermittency of single NC-QDs: Time series of t_{int} = 1 s spectra from (a) aperture A2, d = 820 nm, and (b) A3, d = 630 nm, on the low fluence sample.

false-color representation. In these spectra we identify PL lines labeled A2/3-i. For A2, these lines are centered at E_{A2-1} = 1.837 meV, E_{A2-2} = 1.889 meV, and E_{A2-3} = 1.901 meV, and those for A3 are at E_{A3-1} = 1.827 meV and E_{A3-2} = 1.847 meV. In contrast to the spectra in Figure 4, the line width of these lines is significantly reduced to fwhm ≤0.7 meV and we expect further reduction for even lower optical pump powers as observed also for colloidal QDs at low temperatures.[30] Furthermore, in both time series we observe both random spectral and intensity fluctuations of the isolated sharp emission lines. Such spectral diffusion and luminescence intermittency behaviors are well-known for chemically synthesized colloidal QDs and have been studied together with the underlying mechanisms in great detail since its first observation.[30−33] Most of these models are based on traps surrounding the QD which randomly capture and release photogenerated electrons. Because these processes are uniquely determined by the actual environment of a QD, correlated fluctuations are a clear fingerprint for signals originating from the same emitter. A closer examination of these statistical fluctuations show that signals [A2−2 and A2−3] of A2 and [A3−1 and A3−2] of A3 are clearly correlated. In contrast, there exist no such correlation between A2−1 and [A2−2 and A2−3]. Therefore, these observation provide evidence for the presence of two NC-QDs in A2 and a single NC-QD in A3.

When further comparing the spectral diffusion in panels a and b in Figure 5, different amplitudes and time scales become evident. Each individual emission line exhibits a fast, (sub)-second spectral jitter with an amplitude ranging between $\delta E \approx$ 5 meV (A3−1,A3−2) and $\delta E \approx$ 15 meV (A2−1). These values of δE confirm that spectral diffusion is the dominant contribution to the large linewidths measured for long t_{int} in Figure.4. We attribute the fast jitter as arising from a finite number of defects, such as unsaturated bonds, within the surrounding amorphous SiO_2 matrix. These form a fluctuating background charge that couples to the localized exciton in the NC-QDs. The strength of this coupling mostly determined by the random spatial separation between the individual defects and the CdSe NC-QD. Thus, the different amplitudes of the spectral diffusion, δE, reflect the random positions of the defects. In addition to the spectral diffusion occurring on a (sub)second time scale discussed up to this point, A3−1 and A3−2 exhibit a digital switching. Each emission line remains stable on longer >10 s periods. Such type of behavior could point toward single electron charging and discharging events of an individual defect. At low temperatures, the charge state of the defect is stable on the long time scales observed in our experiment. In contrast, A2−2 and A2−3 do not show such switching on the time scales accessible here, consistent with a fluctuating charge environment in the surrounding matrix, which interacts more weakly with the NC-QD.

CONCLUSIONS

In summary, we demonstrated site-selective ion beam synthesis of CdSe NCs in a SiO_2 matrix using submicrometer implantation masks. The areal density, size and the resulting optical properties were controlled by the implantation fluence and the size of the apertures. For low fluences and small apertures, we reach the regime of individual NC-QDs with confined energy states and discrete emission lines. The optical emission of single NC-QDs exhibit striking similarities to that of colloidal QDs at low temperatures showing both spectral diffusion and intermittency.[30,32] Therefore, we conclude that our ion beam synthesized NC-QDs exhibit optical properties comparable to that of these established QDs synthesized from solution. In single QD experiments, we typically observe emission from less QDs than identified in our SEM characterization. The NC-QDs' optical properties can be further improved adopting passivation strategies established, e.g., for silicon NC-QDs.[14] In particular an increase of the emission intensity would allow to assess the statistics of the emitted photons and confirm single photon emission.[25]

Our approach can be readily extended to nanocomposites of metallic, dielectric or semiconducting NCs in inert dielectric matrices.[9] We expect that the plasmonic, dispersive, and optical properties of these nanocomposites can be tailored adjusting the density and spatial confinement of the implanted stoichiometric constituents, which in turn opens a broad variety of applications. For example, ion beam synthesized II−VI and III−V compound semiconductor NC-QDs are ideally suited as optically active emitters for silicon photonics. Prominent examples of II−VI compound NC-QDs include binary PbS or ternary alloys such as CdS_xSe_{1-x}.[34] While the latter promise additional tunability of the emission wavelength by adjusting the ratio of the group-VI elements, PbS is widely used for near-infrared colloidal QDs emitting at 1.5 μm. Because this wavelength is within the transparency window of silicon and the attenuation minimum of optical fibers, PbS NC-QDs are particularly tantalizing for CMOS integrated silicon photonics and fiber-optical communications. In addition, all types of optically active NC-QDs can be employed as emitters in coupled QD-nanocavity systems when hybridized with SiO_2-based photonic crystal structures.[35] Furthermore, we note that ion beam implantation does not rely in planar substrates. For example, our method can be applied to dope chemically inert, nontoxic SiO_2 micro- and nanospheres with emitters for biomedical applications. The observed pronounced modification of the NCs' structural and optical properties by confining the implantation area to submicrometer dimensions is equally appealing from an material science and solid-state chemistry perspective. It would be particularly interesting to transfer this approach to other types of NCs[9,12,16] and investigate its applicability for the different underlying solid-state chemical reactions.

ASSOCIATED CONTENT

Supporting Information

Raman spectra, TEM of reference sample, high-magnification SEM, full set PL spectra recorded from d = 420 nm apertures of

both samples. This material is available free of charge via the Internet at http://pubs.acs.org/.

AUTHOR INFORMATION

Corresponding Author

*E-mail: hubert.krenner@physik.uni-augsburg.de.

Notes

The authors declare no competing financial interest.

ACKNOWLEDGMENTS

We gratefully acknowledge financial support by the Deutsche Forschungsgemeinschaft (DFG) via the Emmy Noether Program (KR3790/2-1). We thank Achim Wixforth for his continuous support of this project.

REFERENCES

(1) *Ion Beam Modification of Insulators*, Mazzoldi, P.; Arnold, G. W., Eds.; Elsevier: Amsterdam, 1987.

(2) *Ion Beams in Nanoscience and Technology*; Hellborg, R., Whitlow, H. J., Zhang, Y., Eds.; Particle Acceleration and Detection; Springer: Berlin, 2010.

(3) Dennard, R.; Gaensslen, F.; Rideout, V.; Bassous, E.; LeBlanc, A. *IEEE J. Solid-State Circuits* **1974**, *9*, 256−268.

(4) Chason, E.; Picraux, S. T.; Poate, J. M.; Borland, J. O.; Current, M. I.; Diaz de la Rubia, T.; Eaglesham, D. J.; Holland, O. W.; Law, M. E.; Magee, C. W.; Mayer, J. W.; Melngailis, J.; Tasch, A. F. *J. Appl. Phys.* **1997**, *81*, 6513−6561.

(5) Tsukamoto, K.; Kuroi, T.; Kawasaki, Y.; Matsuo, J.; Kase, M.; Aoki, T.; Seki, T. *AIP Conf. Proc.* **2011**, *1321*, 9−16.

(6) Townsend, P. D. *Rep. Prog. Phys.* **1987**, *50*, 501−558.

(7) Polman, A. *J. Appl. Phys.* **1997**, *82*, 1−39.

(8) Meijer, J.; Vogel, T.; Burchard, B.; Rangelow, I.; Bischoff, L.; Wrachtrup, J.; Domhan, M.; Jelezko, F.; Schnitzler, W.; Schulz, S.; Singer, K.; Schmidt-Kaler, F. *Appl. Phys. A: Mater. Sci. Process* **2006**, *83*, 321−327.

(9) Meldrum, A.; Haglund, R. F. J.; Boatner, L. A.; White, C. W. *Adv. Mater. (Weinheim, Ger.)* **2001**, *13*, 1431−1444.

(10) Karl, H.; Großhans, I.; Stritzker, B. *Meas. Sci. Technol.* **2005**, *16*, 32−40.

(11) Lopez, R.; Boatner, L. A.; Haynes, T. E.; Feldman, L. C.; R. F. Haglund, J. *J. Appl. Phys.* **2002**, *92*, 4031−4036.

(12) Zimmer, J.; Wixforth, A.; Karl, H.; Krenner, H. J. *Appl. Phys. Lett.* **2012**, *100*, No. 231911.

(13) Fukumi, K.; Chayahara, A.; Kadono, K.; Sakaguchi, T.; Horino, Y.; Miya, M.; Fujii, K.; Hayakawa, J.; Satou, M. *J. Appl. Phys.* **1994**, *75*, 3075−3080.

(14) Min, K. S.; Shcheglov, K. V.; Yang, C. M.; Atwater, H. A.; Brongersma, M. L.; Polman, A. *Appl. Phys. Lett.* **1996**, *69*, 2033−2035.

(15) Hipp, W.; Karl, H.; Großhans, I.; Stritzker, B. *Mater. Sci. Eng., B* **2003**, *101*, 318−323.

(16) Pavesi, L.; Dal Negro, L.; Mazzoleni, C.; Franzò, G.; Priolo, F. *Nature* **2000**, *408*, 440−444.

(17) Walters, R. J.; Bourianoff, G. I.; Atwater, H. A. *Nat. Mater.* **2005**, *4*, 143−146.

(18) Achtstein, A. W.; Karl, H.; Stritzker, B. *Appl. Phys. Lett.* **2006**, *89*, No. 061103.

(19) Kippenberg, T.; Tchebotareva, A.; Kalkman, J.; Polman, A.; Vahala, K. *Phys. Rev. Lett.* **2009**, *103*, No. 027406.

(20) Ekimov, A.; Efros, A.; Onushchenko, A. *Solid State Commun.* **1985**, *56*, 921−924.

(21) Murray, C. B.; Norris, D. J.; Bawendi, M. G. *J. Am. Chem. Soc.* **1993**, *115*, 8706−8715.

(22) Norris, D. J.; Efros, A. L.; Erwin, S. C. *Science* **2008**, *319*, 1776−1779.

(23) Klostranec, J.; Chan, W. *Adv. Mater. (Weinheim, Ger.)* **2006**, *18*, 1953−1964.

(24) Kramer, I. J.; Sargent, E. H. *ACS Nano* **2011**, *5*, 8506−8514.

(25) Michler, P.; Imamoglu, A.; Mason, M.; Carson, P.; Strouse, G.; Buratto, S. *Nature* **2000**, *406*, 968−970.

(26) Norris, D.; Bawendi, M. *Phys. Rev. B* **1996**, *53*, 16338−16346.

(27) Efros, A. L.; Rosen, M. *Phys. Rev. B* **1998**, *58*, 7120−7135.

(28) Trallero-Giner, C.; Debernardi, A.; Cardona, M.; Menéndez-Proupn, E.; Ekimov, A. *Phys. Rev. B* **1998**, *57*, 4664−4669.

(29) Yu, W. W.; Qu, L.; Guo, W.; Peng, X. *Chem. Mater.* **2003**, *15*, 2854−2860.

(30) Empedocles, S.; Norris, D.; Bawendi, M. *Phys. Rev. Lett.* **1996**, *77*, 3873−3876.

(31) Nirmal, M.; Dabbousi, B. O.; Bawendi, M. G.; Macklin, J. J.; Trautman, J. K.; Harris, T. D.; Brus, L. E. *Nature* **1996**, *383*, 802−804.

(32) Neuhauser, R.; Shimizu, K.; Woo, W.; Empedoclesqq, S.; Bawendi, M. *Phys. Rev. Lett.* **2000**, *85*, 3301−3304.

(33) Frantsuzov, P.; Kuno, M.; Jankó, B.; Marcus, R. A. *Nat. Phys.* **2008**, *4*, 519−522.

(34) Huber, P.; Karl, H.; Lindner, J.; Stritzker, B. *Nucl. Instrum. Methods Phys. Res., Sect. B* **2006**, *242*, 170−172.

(35) Gong, Y.; Ishikawa, S.; Cheng, S.-L.; Gunji, M.; Nishi, Y.; Vučković, J. *Phys. Rev. B* **2010**, *81*, No. 235317.